analytical chemistry

pubs.acs.org/ac Article

Optical Microfiber with a Gold Nanorods–Black Phosphorous Nanointerface: An Ultrasensitive Biosensor and Nanotherapy Platform

He Liang,[‖] Luyan Zhou,[‖] Pengwei Chen,[‖] Jiaying Zheng, Yunyun Huang,* Jiaxuan Liang, Junyang Zhong, Yugang Huang, Mingguang Yu, and Bai-Ou Guan*

Cite This: *Anal. Chem.* 2022, 94, 8058–8065 Read Online

ACCESS | Metrics & More | Article Recommendations | Supporting Information

ABSTRACT: The detection and therapy of cancers in the early stage significantly alleviate the associated dangers. Optical devices offer new opportunities for these early measures. However, the clinical translation of the existing methods is severely hindered by their relatively low sensitivity or unclear physiological metabolism. Here, an optical microfiber sensor with a drug loading gold nanorod–black phosphorous nanointerface, as an ultrasensitive biosensor and nanotherapy platform, is developed to meet the early-stage requirement. With interface sensitization and functionalization of the hybrid nanointerface, the microfiber sensor presents an ultrahigh sensing performance, achieving the selective detection of the HER2 biomarker with limits of detection of 0.66 aM in buffer solution and 0.77 aM in 10% serum. It can also distinguish breast cancer cells from other cells in the early stage. Additionally, enabled by the interface, the optical microfiber is able to realize cellular nanotherapy, including photothermal/chemotherapy with pump laser coupling after diagnosis, and evaluate therapy results in real time. The immobilization of the interface on the optical microfiber surface prevents the damage to normal cells induced by nanomaterial enrichment, making the device more efficient and intelligent. This study opens up a new avenue for the development of smart optical platforms for sensitive biosensing and precision therapy.

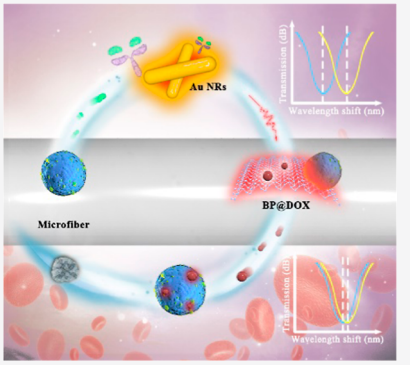

INTRODUCTION

The early diagnosis and treatment of cancers can significantly alleviate the damage.[1] An approach integrating sensing and therapy functions could provide early warning, accurate therapy, and the evaluation of healing effects in the early stages of cancers. Such a strategy buys time for tumor treatment. In recent years, the development of nanomaterials for cost-effective precision medicine has attracted increasing attention.[2−4] A series of exciting diagnosis strategies, including magnetic resonance imaging,[5] ultrasound,[6] and optical methods,[7−9] have been integrated into theranostics with therapeutic processes.[10−12] Despite encouraging progress, in the early stage of cancer, the concentrations of biomarkers are ultralow. Diagnosis in this stage requires a sensor with ultrahigh sensitivity. Moreover, the therapy particles injected into blood vessels may accumulate in the body and cause injury to normal cells.[13−15] Therapies with good localization and accuracy are in great demand. Consequently, a flexible cancer detection and therapy platform integrating ultrasensitive biosensing and precise nanotherapy is highly required in the early stage of disease.

Phototheranostics has become one of the most prospective strategies in this field.[16] Optical microfibers, with the features of low cost and flexibility,[17] have been widely employed as biosensors.[18,19] If the therapy elements can also be immobilized on a surface and trigger the nanotherapy at the locations where excessive biomarkers are detected, accidental injury to normal cells might be avoided. Its operation wavelength in the near-infrared (NIR) range ensures the penetration of light in vivo and reduces harm to the body.[20] However, the relatively low sensitivity hinders utility of the sensing application in the early stages.[21] Its silica surface also presents obstacles in nanotherapeutic integration. The construction of a nanointerface is an effective approach for a solution.[22] Two-dimensional (2D) nanomaterials, with unique planar topography, have attracted great attention in the application of nanotherapy.[23] They have also been demonstrated as nanointerface materials on optical microfibers to enlarge the assembly surface area[22] and to support plasmonic materials as spacers to improve the sensitivity of sensors.[24] Among this large family, black phosphorous (BP), with its large NIR extinction coefficient, high photothermal conversion

Received: April 6, 2022
Accepted: May 11, 2022
Published: May 25, 2022

https://doi.org/10.1021/acs.analchem.2c01499
Anal. Chem. 2022, 94, 8058–8065

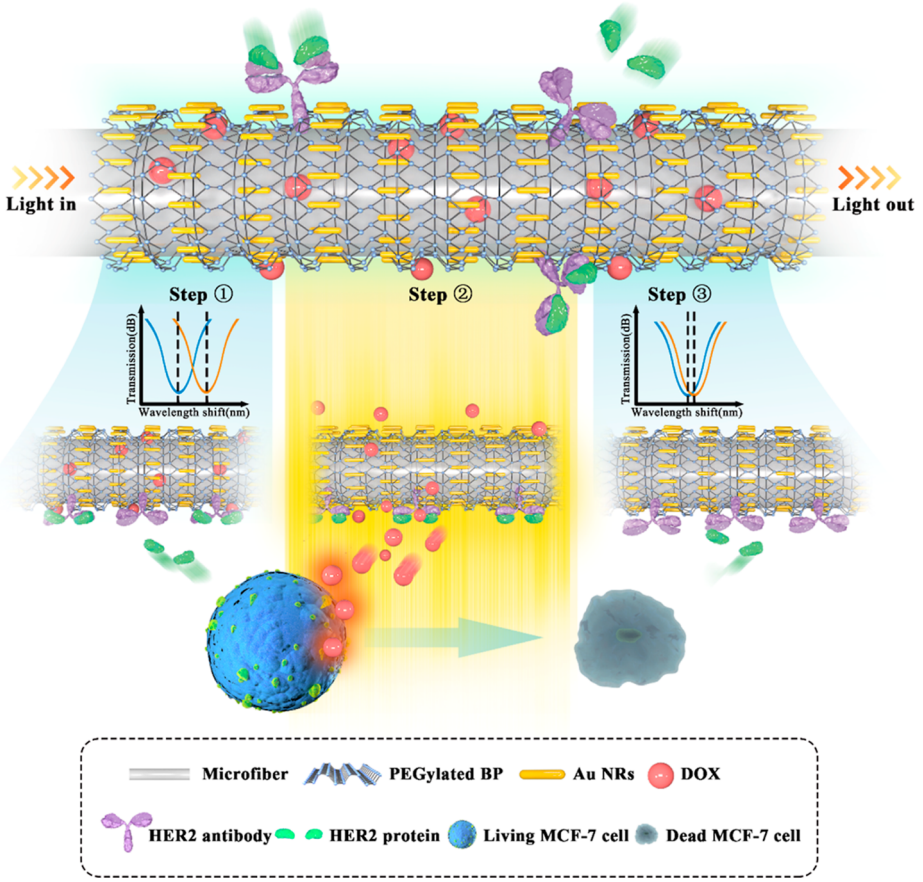

Figure 1. Sketch showing the Au-DOX@BP interface-functionalized optical microfiber sensor for the detection of HER2 biomarkers and cellular nanotherapy.

efficiency, and good biocompatibility,[25−27] presents good potential for ultrasensitive biosensor and nanotherapeutic platform integration.

In this work, an optical microfiber as an ultrasensitive biosensor and nanotherapy platform was realized through nanointerface functionalization. A nanointerface made of BP nanosheet-supporting gold nanorods (Au NRs) was constructed on the optical microfiber, as shown in Figure 1. The BP nanosheets, loaded with an anticancer drug (doxorubicin, DOX), were used to establish a nanotherapy system for synergistic cellular photothermal/chemotherapy of cancer. Meanwhile, to optimize the plasmonic electromagnetic field enhancement, these BP nanosheets were employed as a spacer to support the Au NRs.[28] The Au NRs on BP nanosheets improved the microfiber's sensitivity through the electromagnetic field enhancement of the evanescent field and triggered the drug delivery through their plasmonic photothermal effect synergized with the BP nanosheets.[29] Furthermore, the absorption wavelength of Au NRs coincided with that of the pump source at 980 nm, which could better stimulate the photothermal and chemotherapy effects of the sensor interface. Therefore, in this work, Au NRs were chosen to construct the sensor interface. With the evanescent field enhancement by the Au-DOX@BP nanointerface, the optical microfiber presented a high sensing performance with a limit of detection (LOD) of 0.66 aM for the HER2 protein (the human epidermal growth factor receptor 2[30]). It was capable of detecting breast cancer cells in the early stage. The nanointerface endowed the nanotherapy function with the microfiber, and it is also capable of evaluating the therapy results in real time. By restricting the sensing agents and the nanocapsules on the interface, damage to normal cells caused by metabolic nanomaterial enrichment is avoided as much as possible. These findings may establish an alternative and easy-to-use approach for the in situ integration of diagnosis, nanotherapy, and healing effect evaluation in the early stages of disease.

EXPERIMENTAL SECTION

Nanointerface Functionalization. The silica microfiber was hydroxylated through immersing in a bath with piranha solution for 30 min. Following, an immersion of microfiber in the 3-aminopropyl-triethoxysilane solution was carried out and then washed with ethanol thoroughly following our previous work.[24] After that, the aminated microfiber was dipped in the DOX@PEGylated BP dispersion (0.0625 mg/mL) for 30 min before pulling out and washing with deionized water and ethanol. Finally, the microfiber with DOX@PEGylated BP-nanointerface was immersed in the amino-modified Au NR dispersion (0.0333 mg/mL) for 20 min before pulling out and washing with deionized water and ethanol.

For other experimental details, please see the Supporting Information.

RESULTS

Nanointerface Design and Functionalization. To increase the biocompatibility and stability of the BP spacer, it was modified by polyethylene glycol-amine (PEG-NH_2).[31,32]

https://doi.org/10.1021/acs.analchem.2c01499
Anal. Chem. 2022, 94, 8058−8065

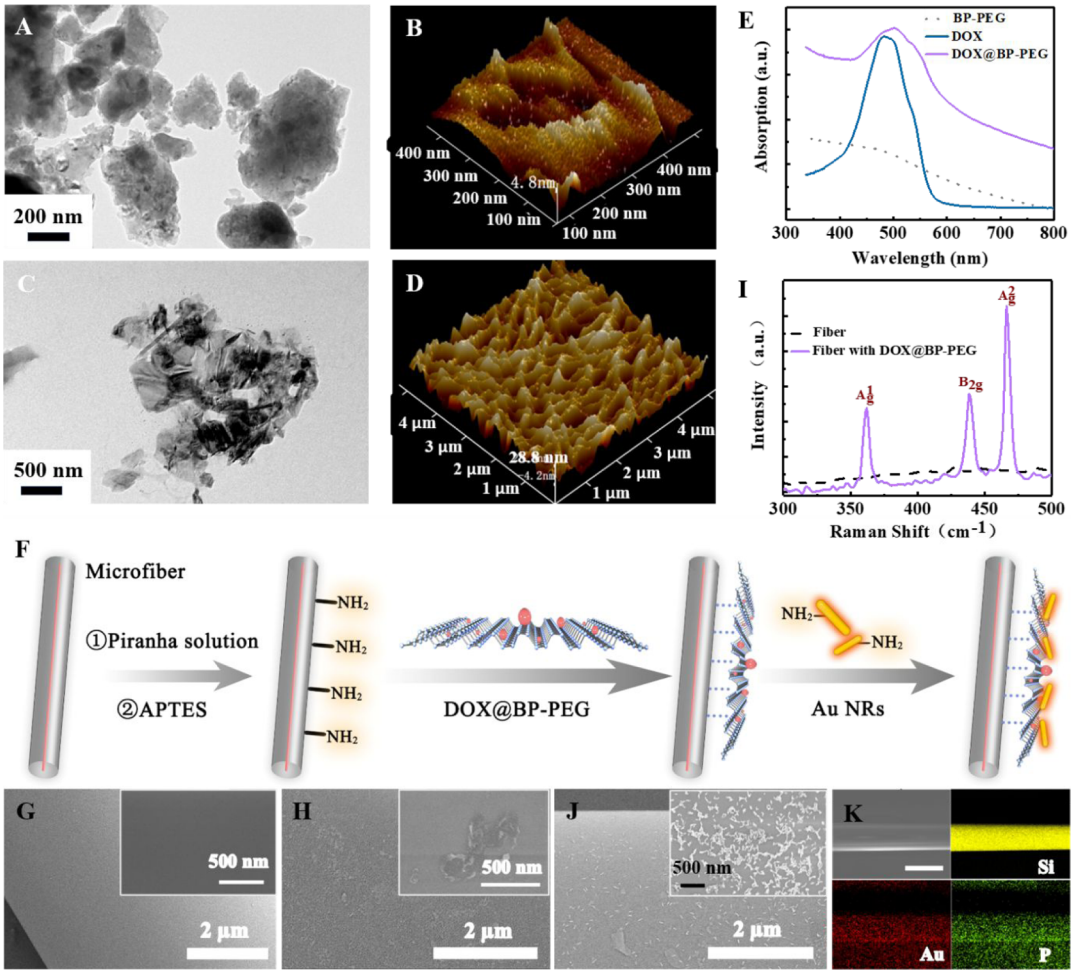

Figure 2. Nanointerface design. (A) TEM and (B) AFM images of PEGylated BP. (C) TEM and (D) AFM images of DOX@PEGylated BP. (E) UV−vis absorption spectra of PEGylated BP, DOX, and DOX@PEGylated BP. (F) Schematic of the nanointerface functionalization of microfiber. SEM images of the (G) silica microfiber surface and (H) microfiber with DOX@PEGylated BP nanosheets. (I) Raman spectra of the silica microfiber and the surface of microfiber with the PEGylated BP interface. (J) SEM image and (K) EDS mapping of the microfiber surface with the Au-DOX@BP interface (insets of G,H,J: zooms of microfiber surfaces. The scale bar in Figure 2K is 50 nm. The fiber used here was larger in size because of the resolution of the instrument. As the thicknesses of Au NRs and BP were very thin compared with SiO_2, their signals were affected by the substrate noise to a certain extent).

Thereafter, the surface of the PEGylated BP nanosheets was loaded with DOX for chemotherapy.[26,27] Transmission electron microscopy (TEM) and atomic force microscopy (AFM) were performed to characterize the morphology of the PEGylated BP nanosheets and the DOX-loaded PEGylated BP nanosheets (DOX@PEGylated BP) (Figures 2A−D and S1). The lateral size of the modified BP nanosheets was ∼300 nm (Figure 2A) with a thickness of ∼3 nm (Figures 2B and S1A,B), indicating that they consisted of three layers. After DOX loading, an identifiable rough surface with an increased thickness of ∼15 nm could be observed (Figures 2C,D and S1C−D). The UV−vis absorption spectrum of the DOX@PEGylated BP sheets (Figure 2E) showed an obvious DOX absorption peak,[33,34] indicating the DOX loading. The DOX loading capacity of the PEGylated BP nanosheets was evaluated using UV−vis spectroscopic analysis (Figure S2), and the results showed a loading content (LC) of ∼120%. In addition to the DOX@PEGylated BP nanosheets, Au NRs with a length-to-diameter ratio of 10 (Figure S3) were prepared for assembly on the optical microfiber interface.

A silica optical biconical microfiber, consisting of a diameter-decreasing transition region, a waist region of 7.1 μm in diameter and 1.85 mm in length, and a diameter-increasing transition region (Figure S4), was employed as a transducer. Interacting with the surface matter through the evanescent field, the fiber spectrum red-shifts as the surface refractive index increases.[22] A series of surface modifications and electrostatic attractions[24,35] enabled the assembly of the DOX@PEGylated BP nanosheets and Au NR interfaces on the silica optical microfiber, as shown in Figure 2F. The DOX@PEGylated BP functionalization was confirmed by the scanning electron microscopy (SEM) images, as shown in Figure 2G,H, and the Raman spectra, as shown in Figures 2I and S5. The smooth surface of the silica microfiber, as observed in Figure 2G, increased the difficulty of Au NR and antibody immobilization. The uniform distribution of BP on the microfiber surface, as observed in Figure 2H, increased the surface area, which was conducive to the assembly of Au NRs and the subsequent antibody. The characteristic Raman peaks of BP on the microfiber surface (Figure 2I) also indicate the modification of BP on the interface. On this basis, Au NRs with amino groups were immobilized on the electronegative DOX@PEGylated BP nanosheet surface through electrostatic attraction,[36] forming the Au-DOX@BP interface. The SEM

https://doi.org/10.1021/acs.analchem.2c01499
Anal. Chem. 2022, 94, 8058−8065

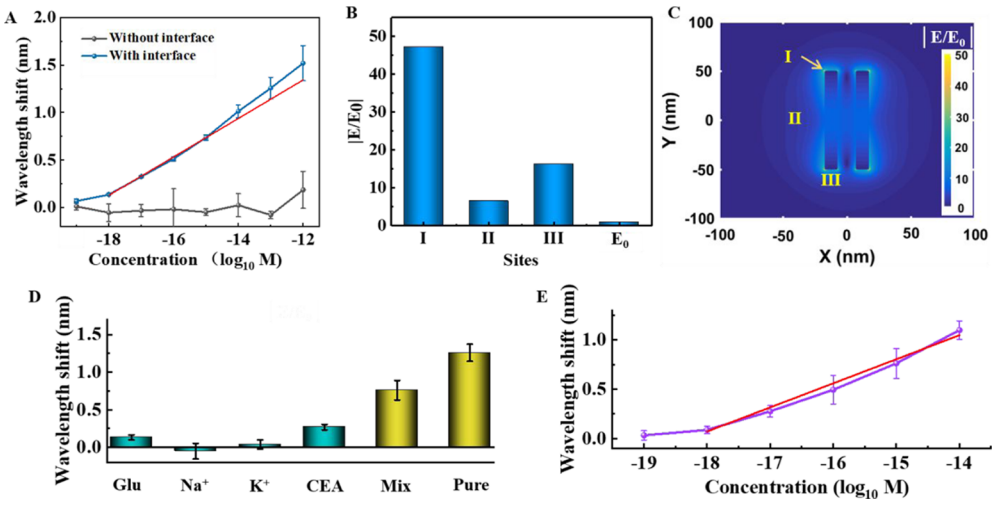

Figure 3. HER2 detection ability. (A) Wavelength shift responses of the as-prepared sensor and the control sensor to different HER2 concentrations. (B) Localized electric field enhancement of the microfiber surface at different sites. (C) Calculated near-field intensity mapping of the microfiber surface functionalized with the Au-DOX@BP nanointerface. (D) Optical responses of the sensor to 0.1 pM HER2 solution and other potential interferents at high concentrations (Na^+: 1 μM; K^+: 1 μM; glucose: 1 μM; and carcinoembryonic antigen: 0.1 pM; the mixture contained the above interferents and 0.1 pM HER2 antigens). (E) Wavelength shifts of the as-prepared sensor to different HER2 concentrations in 10% serum.

image in Figure 2J and the energy-dispersive X-ray spectroscopy (EDS) mapping in Figure 2K confirm the Au-DOX@BP interface construction on the microfiber. As demonstrated in the SEM images of the microfiber surface in Figure S6 and the statistical results in Table S1, Au NRs occupied 22.30% of the surface area of the microfiber. After the construction of the interface, the optical microfiber was made ready for sensing via the immobilization of HER2 antibodies. Its surface morphology is shown in Figure S7.

Protein Biomarker Sensing. Figure 3 shows the results of the evaluation of the sensing ability of the as-prepared sensor against HER2 antigens. A control sensor without an interface and with HER2 antibodies directly immobilized on the silica microfiber surface was employed to investigate the role of the Au-DOX@BP interface. As shown in Figures 3A and S8, an increase in the HER2 antigen concentration from 1 aM to 1 pM resulted in regular red-shifts of 202 pm/$\log_{10}$ M in the transmission spectrum of the as-prepared sensor [since the concentration of anti-HER2 antibody immobilized on the microfiber surface was 10^{-8} M, the detection capability of sensor got to a saturation when the concentration of HER2 solution reached 10^{-8} M (Figure S9)]. The detection result, as obtained in Figure 3A, was the average of three independent tests. The small error bars demonstrate the sensor's reproducibility. Based on the spectrum variation of the sensor in PBS solution (Figure S10), its LOD (signal/noise ratio $\geq$ 3)[24] reached 0.66 aM. Table S2 compares the key performance of this biosensor with some recently reported HER2 biosensors. This sensor was more than 2 orders lower than those of previously reported methods.[37−39] As a control, the sensor without an interface presented a sensing ability that was obviously weaker than that of the sensor with an interface and could only detect the target molecules at concentrations higher than 1 pM. Therefore, the sensor with the Au-DOX@BP nanointerface showed a linearity range from 1 aM to 1 pM with an LOD approximately 7 orders of magnitude lower than that of the sensor without the interface, thus establishing the nanointerface as a key player in improving the sensor sensitivity. Even more interesting is that, by comparing Figures S10 and S11, the Au-DOX@BP nanointerface makes the microfiber sensor more stable in solution. Thus, it improves the sensitivity and stability of the sensor.

A penetration depth[40,41] of ~1 μm was obtained for an optical microfiber at this size (Figure S12). A finite-difference time-domain approach was performed to demonstrate the electric field enhancement of microfiber surfaces with the Au-DOX@BP nanointerface [$|E/E_0|$, which is the ratio of the enhanced electric field (E) to the initial one, that is, that of the silica microfiber surface without interface (E_0)], as shown in Figure 3B,C. The strongest electric field enhancement of the Au-DOX@BP-functionalized microfiber surface in the wavelength range of the evanescent field between 1250 and 1650 nm (Figure 3C) was approximately 50-fold higher than that of the microfiber surface without an interface. These results are due to the synergistic electromagnetic field enhancement of Au NRs assisted by the BP spacer.[42,43] Given that the microfiber here was applied as a wavelength-encoded sensor, the sensitivity is proportional to the fiber surface energy on the target-binding sites,[44] that is, $|E(x, y)|^2$. This result is equal to the square of the electric field enhancement of the microfiber surface with the Au-DOX@BP nanointerface ($|E/E_0|^2$), which was found to be ~2500-fold higher than that of the sensor without the interface. Furthermore, the localized enhancement property of the plasmon nanointerface confined the electromagnetic field improvement on the microfiber surface, which was the site of the immobilized antigen−protein conjugate. Different from the uniform enhancement of the entire evanescent field, it only enhanced the signal caused by the binding of the targets but not the signal induced by interference in the solution. This improved the signal-to-noise ratio, which is beneficial to the application of microfiber sensors in real samples with complex compositions.

To evaluate the sensing ability in real samples, the optical responses of the sensor to interfering molecules that might exist at a relatively high concentration were considered (Figure 3D). Only HER2 proteins induced a notable optical wavelength red-shift through the as-prepared sensor; other substances caused no obvious optical responses even though

https://doi.org/10.1021/acs.analchem.2c01499
Anal. Chem. 2022, 94, 8058−8065

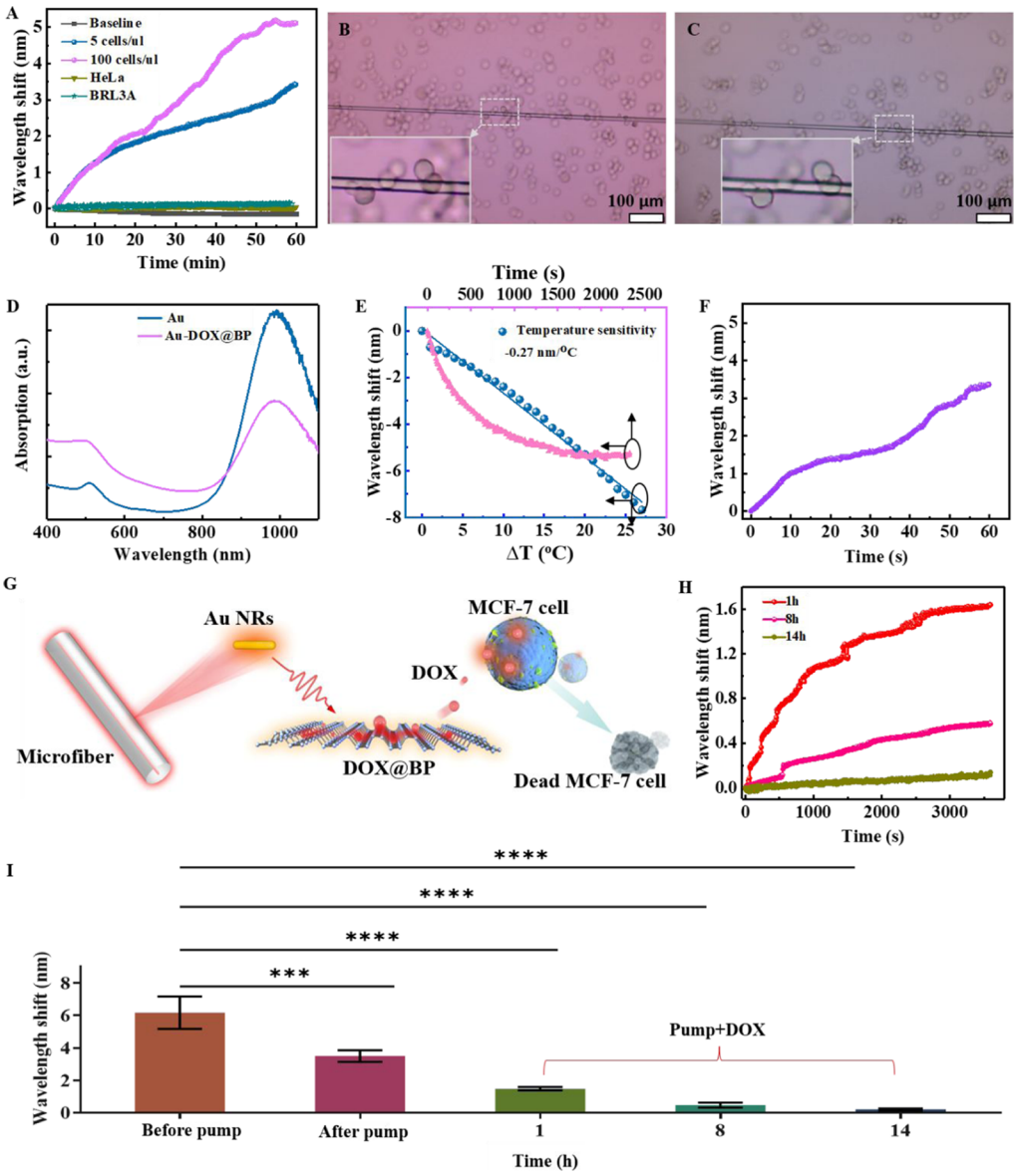

Figure 4. In situ monitoring of HER2 antigens in cells. (A) Optical wavelength shift responses of the as-prepared sensor to the culture medium, MCF-7 cells at 5 and 100 cells/μL concentrations, HeLa cells at 100 cells/μL, and BRL3A cells at 100 cells/μL. (B) Optical microscopy images of the sensor capturing MCF-7 cells. (C) Optical microscopy images of the sensor surface washed with PBS solution after capturing MCF-7 cells. [Insets of (B,C): zooms of the cells immobilized on the fiber surface.] (D) UV−vis absorption spectra of Au and Au-DOX@BP. (E) Temperature sensitivity of the optical microfiber with Au@BP and wavelength shift of the microfiber with the Au−BP nanointerface under pump laser coupling (blue plots: wavelength shifts with the surrounding temperature increase. The fiber surrounding was heated by a water bath, and the temperature was calibrated by a thermocouple. It was linearly fitted to obtain a temperature sensitivity of −0.27 nm/°C. Pink plots: wavelength shift with time of the microfiber with the Au−BP nanointerface under pump laser coupling. Its total wavelength shift was ∼5.4 nm, corresponding to ∼20 °C). (F) Optical response in MCF-7 cells after pumping and heating for 30 min. (G) Schematic diagram of the drug delivery process triggered by the laser irradiation in the microfiber. (H) Optical response in MCF-7 cells (100 cells/μL) after the synergistic effect of pump heating and DOX therapy. (I) Wavelength shifts of the as-prepared sensor to MCF-7 cells before pump heating, after isolated photothermal therapy, and after the synergistic effect of pump heating and DOX therapy for 1, 8, and 14 h (the error bars represent the standard deviations of three independent tests. ***P = 0.0002 and ****P < 0.0001).

the concentrations were 7 orders of magnitude higher than that of the target protein. Additionally, in a mixture of HER2 proteins at a low concentration (0.1 pM) and other interfering molecules at high concentrations, the sensor displayed a response similar to that observed in the absence of the interfering molecules, demonstrating its specificity. Figures 3E and S13 present sensor responses to HER2 antigens at different concentrations in a 10% serum solution. A regular transmission red-shift with a sensitivity of 245 pm/$\log_{10}$ M was recorded by the sensor when HER2 concentrations increased from 1 aM to 10 fM. Based on the sensor noise in 10% serum (Figure S14), the LOD was estimated to be 0.77 aM. The energy loss caused by the various interfering tissues[45] in the serum did not significantly reduce the sensitivity. This result demonstrates the advantages of the microfiber sensor with the Au-DOX@BP nanointerface in the detection of samples with complex components. Thus, the as-prepared sensor was ready for in situ cell monitoring.

https://doi.org/10.1021/acs.analchem.2c01499
Anal. Chem. 2022, 94, 8058−8065

Distinguishing Breast Cancer Cells. As shown in Figures 4A−C, S15, and S16, the as-prepared sensor was utilized to distinguish breast cancer cells from other cells. MCF-7 cells (the breast cancer cell line primarily used in breast cancer research)[46] were used as the target cancer cells, and the HeLa cell line[47] and BRL3A cells (a normal rat liver cell line) were used as the control cells. The expression level of HER2 proteins on the MCF-7-cell surface has been reported to be much higher;[48] thus, MCF-7 cells could be captured on the sensor surface through the binding reaction between HER2 proteins on the cell surface and antibodies on the sensor surface.[37] As shown in the optical microscopy images in Figures S15 and 4B−C, when the cell culture solution of MCF-7 cells (100 cells/μL) was injected, the sensor captured the cells on its surface within the first 10 min. After 30 min, the number of cells bound on the sensor surface increased markedly. Then, PBS solution was injected to wash the sensor surface. As presented in Figure 4C and Video S1, after three washes, the MCF-7 cells were still captured on the microfiber surface, demonstrating that the cells were bound to the sensor surface by the antigen−antibody reaction rather than by adhesion.

This optical responses to the MCF-7 cells (100 and 5 cells/μL) are recorded, as shown in Figure 4A, accompanied by the responses to the culture medium (baseline), the control groups (HeLa cells at a density of 100 cells/μL and BRL3A cells at a density of 100 cells/μL). After exposure to MCF-7 cells at a density of 100 cells/μL, a dramatic red-shift was recorded in the first 10 min. The wavelength shift leveled off after 50 min. This result is consistent with the binding process of MCF-7 cells on the microfiber surface observed under the microscope (Figure S15). For the MCF-7 cells at a lower concentration of 5 cells/μL, the sensor recorded a smaller wavelength shift. For the baseline group and the control groups, which were HeLa cells and BRL3A cells, the sensor recorded no obvious wavelength shift. The microscopy images confirm the optical response of the sensor to HeLa cells. Few cells were captured on the microfiber surface in 30 min (Figure S16). The few HeLa cells floating across the microfiber surface also disappeared after washing the surface with PBS solution. This result indicates that the as-prepared sensor captured MCF-7 cells via the HER2 proteins on the surface of cancer cells, which gave it the ability to distinguish breast cancer cells from other cells. However, since the sensor was sensitive to temperature and strain, the real in vivo detection application will need temperature correction and device packaging.

Nanotherapy. It has been reported that localized hyperthermia can be realized by an optically powered fiber-optic device.[49] To generate the photothermal effect of the nanointerface, a pump laser at 980 nm was coupled into the microfiber. The Au NRs on the microfiber interface presented an absorption peak at 980 nm (Figure 4D). The photothermal effect of the interface was excited through the synergistic effect of Au NRs and BP nanosheets.[36] As shown in Figure 4E, the microfiber with the Au@BP nanointerface presented a temperature sensitivity of −0.27 nm/°C. Accordingly, the temperature of the nanointerface increased by ∼20 °C within 30 min with pump laser coupling. This temperature would be 57 °C when applied in vivo. Although the silica microfiber without the interface and microfiber with the BP interface could also generate photothermal effects under the pump laser, the heating effects were weaker than that of the microfiber with the Au@BP nanointerface (Figure S17). Thus, the microfiber with Au@BP nanointerface could kill the captured cancer cells on its surface via the photothermal effect.[36]

The Au−BP interface without DOX loading was used to verify the photothermal efficacy of the interface independently (excluding the effect of drug delivery). After pumping and heating for 30 min, the sensor was employed to detect the MCF-7 cell concentration again. The concentration of cancer cells was significantly lower than that before photothermal therapy (Figure 4F). Optical microscopy images of the sensor surface in MCF-7 cells after pump on were obtained to reveal the photothermal therapy process to cells, as shown in Figure S18. The photothermal effect of the microfiber interface not only could heat and kill the cells captured on its surface but could also attract nearby cells and kill them within 30 min, demonstrating that the photothermal effect of the interface played an important role in the killing of cancer cells before the drug took effect. This led to a sharp decrease in the number of breast cancer cells around the sensor.

For the Au-DOX@BP nanointerface, the effective photothermal heating property of the nanointerface stimulated enhanced DOX release upon NIR irradiation (Figure 4G). The DOX release effect was determined and is shown in Figure S19. The nanotherapy results were then evaluated using the microfiber sensor (Figure 4H). Exposed to the cancer cells, the transmission spectrum of the sensor showed a red-shift (∼1.6 nm) 1 h after 30 min of NIR irradiation, which was obviously smaller than that before irradiation (∼6 nm), as shown in Figure 4A, and the results recorded after isolated photothermal therapy (∼3 nm) are shown in Figure 4F. As the time after irradiation increased, the wavelength shift recorded by the sensor decreased. By the 14th hour, the recorded wavelength shift tended to 0, suggesting that over this period, the number of cancer cells had been dramatically decreased. According to the optical response, as shown in Figures 4I and S20−S24, the sensor could effectively distinguish between the cancer cell densities before therapy and after photothermal therapy (P = 0.0002) and that before therapy and after photothermal/DOX therapy (P < 0.0001). This result establishes the synergistic effect of photothermal/chemotherapy at the cellular level. Thus, the as-prepared sensor showed potential for applications in multimodal therapy and therapy result evaluation in situ and in real time.

CONCLUSIONS

To meet the requirements of early-stage cancer detection and therapy, an optical microfiber sensor has been employed through nanointerface design. An Au NRs-DOX@BP nanointerface that integrates an ultrahigh sensing performance and a nanotherapy function to realize detection and therapy while avoiding the accidental injury of normal cells caused by the diffusion of nanomaterials into body metabolism was developed on the microfiber. With the evanescent field enhancement of the nanointerface, the microfiber, as an ultrasensitive biosensor, achieved selective HER2 protein detection with LODs of 0.66 aM in buffer solution and 0.77 aM in 10% serum, meeting the requirements of detecting trace concentrations of biomarkers in the early stage. It could also differentiate breast cancer cells from other cells. The interface, which could increase the surface temperature to 57 °C in vivo, similar to a nanocapsule for anticancer drugs, gives the sensor the ability to realize photothermal therapy and drug delivery after diagnosis and evaluate the therapy results in real time. Additionally, the microfiber avoids damage to normal cells

https://doi.org/10.1021/acs.analchem.2c01499
Anal. Chem. 2022, 94, 8058−8065

caused by metabolic nanomaterial enrichment. The integration of detection and nanotherapeutic functions on a microscale-sized optical probe makes it more compact, efficient, and intelligent. Therefore, this work paves the way for the design of smart platforms for sensitive biosensing and precise therapy in the early stages of cancer.

■ ASSOCIATED CONTENT

Supporting Information

The Supporting Information is available free of charge at https://pubs.acs.org/doi/10.1021/acs.analchem.2c01499.

Video of MCF-7 cells captured on microfiber surface (AVI)

Experimental details; AFM images of nanosheets; DOX loading content determination; TEM images of the Au NRs; optical microscopy photograph of the microfiber; Raman spectra of the microfiber surface with BP, DOX, and PEG; SEM image of the microfiber with HER2 antibodies on the nanointerface; wavelength variation of the as-prepared sensor in PBS solution and serum; comparison of analytic parameters of the HER2 biosensors; transverse electric field amplitude distributions of the HE_{12} mode; optical microscopy images; confocal laser scanning microscopy images; and measured transmission spectra (PDF)

■ AUTHOR INFORMATION

Corresponding Authors

Yunyun Huang − *Guangdong Provincial Key Laboratory of Optical Fiber Sensing and Communications, Institute of Photonics Technology, Jinan University, Guangzhou 511143, China;* orcid.org/0000-0001-7528-1001; Email: thuangyy6@jnu.edu.cn

Bai-Ou Guan − *Guangdong Provincial Key Laboratory of Optical Fiber Sensing and Communications, Institute of Photonics Technology, Jinan University, Guangzhou 511143, China;* orcid.org/0000-0002-3790-2986; Phone: 20-37336640; Email: tguanbo@jnu.edu.cn

Authors

He Liang − *Guangdong Provincial Key Laboratory of Optical Fiber Sensing and Communications, Institute of Photonics Technology, Jinan University, Guangzhou 511143, China*

Luyan Zhou − *Guangdong Provincial Key Laboratory of Optical Fiber Sensing and Communications, Institute of Photonics Technology, Jinan University, Guangzhou 511143, China*

Pengwei Chen − *Guangdong Provincial Key Laboratory of Optical Fiber Sensing and Communications, Institute of Photonics Technology, Jinan University, Guangzhou 511143, China*

Jiaying Zheng − *Guangdong Provincial Key Laboratory of Optical Fiber Sensing and Communications, Institute of Photonics Technology, Jinan University, Guangzhou 511143, China*

Jiaxuan Liang − *Guangdong Provincial Key Laboratory of Optical Fiber Sensing and Communications, Institute of Photonics Technology, Jinan University, Guangzhou 511143, China*

Junyang Zhong − *School of Pharmaceutical Sciences, Guangzhou Medical University, Guangzhou 511436, China*

Yugang Huang − *School of Pharmaceutical Sciences, Guangzhou Medical University, Guangzhou 511436, China;* orcid.org/0000-0001-8883-2431

Mingguang Yu − *School of Materials Science and Energy Engineering, Foshan University, Foshan 528000, China*

Complete contact information is available at: https://pubs.acs.org/10.1021/acs.analchem.2c01499

Author Contributions

[‖]H.L., L.Z., and P.C. contributed equally to this work.

Notes

The authors declare no competing financial interest.

■ ACKNOWLEDGMENTS

The authors thank the support from the National Natural Science Foundation of China (nos. 51773084, U1701268, and 51403043), the Natural Science Foundation of Guangdong Province (no. 2019A1515011278), the Local Innovative and Research Teams Project of Guangdong Pearl River Talents Program (no. 2019BT02X105), the Guangzhou Science and Technology Plan Project (no. 201904020032), the Fundamental Research Funds for the Central Universities (no. 21617420), the Special Funds for the Cultivation of Guangdong College Students' Scientific and Technological Innovation (Climbing Program Special Funds, no. pdjh2020a0061), the Undergraduate Innovation and Entrepreneurship Program (no. 202010559050), and the Open Funding of Foshan University. We would like to thank A.J.E. for English language editing.

■ REFERENCES

(1) Litwin, M. S.; Tan, H.-J. *JAMA* **2017**, *317*, 2532−2542.
(2) Jokerst, J. V.; Gambhir, S. S. *Acc. Chem. Res.* **2011**, *44*, 1050−1060.
(3) Pei, H.; Zuo, X.; Zhu, D.; Huang, Q.; Fan, C. *Acc. Chem. Res.* **2014**, *47*, 550−559.
(4) Lyu, Y.; Fang, Y.; Miao, Q.; Zhen, X.; Ding, D.; Pu, K. *ACS Nano* **2016**, *10*, 4472−4481.
(5) Yang, K.; Yang, G.; Chen, L.; Cheng, L.; Wang, L.; Ge, C.; Liu, Z. *Biomaterials* **2015**, *38*, 1−9.
(6) Wang, X.; Niu, D.; Li, P.; Wu, Q.; Bo, X.; Liu, B.; Bao, S.; Su, T.; Xu, H.; Wang, Q. *ACS Nano* **2015**, *9*, 5646−5656.
(7) Huang, P.; Lin, J.; Wang, X.; Wang, Z.; Zhang, C.; He, M.; Wang, K.; Chen, F.; Li, Z.; Shen, G.; Cui, D.; Chen, X. *Adv. Mater.* **2012**, *24*, 5104−5110.
(8) Ge, J.; Jia, Q.; Liu, W.; Guo, L.; Liu, Q.; Lan, M.; Zhang, H.; Meng, X.; Wang, P. *Adv. Mater.* **2015**, *27*, 4169−4177.
(9) Ai, X.; Ho, C. J. H.; Aw, J.; Attia, A. B. E.; Mu, J.; Wang, Y.; Wang, X.; Wang, Y.; Liu, X.; Chen, H.; Gao, M.; Chen, X.; Yeow, E. K. L.; Liu, G.; Olivo, M.; Xing, B. *Nat. Commun.* **2016**, *7*, 10432.
(10) Chen, Q.; Xu, L.; Liang, C.; Wang, C.; Peng, R.; Liu, Z. *Nat. Commun.* **2016**, *7*, 13193.
(11) Abbas, M.; Zou, Q.; Li, S.; Yan, X. *Adv. Mater.* **2017**, *29*, 1605021.
(12) Zeng, X.; Luo, M.; Liu, G.; Wang, X.; Tao, W.; Lin, Y.; Ji, X.; Nie, L.; Mei, L. *Adv. Sci.* **2018**, *5*, 1800510.
(13) Kam, N. W. S.; O'Connell, M.; Wisdom, J. A.; Dai, H. *Proc. Natl. Acad. Sci. U.S.A.* **2005**, *102*, 11600−11605.
(14) Seo, W. S.; Lee, J. H.; Sun, X.; Suzuki, Y.; Mann, D.; Liu, Z.; Terashima, M.; Yang, P. C.; McConnell, M. V.; Nishimura, D. G.; Dai, H. *Nat. Mater.* **2006**, *5*, 971−976.
(15) Robinson, J. T.; Tabakman, S. M.; Liang, Y.; Wang, H.; Casalongue, H.; Vinh, D.; Dai, H. *J. Am. Chem. Soc.* **2011**, *133*, 6825−6831.

(16) Chen, H.; Zhang, W.; Zhu, G.; Xie, J.; Chen, X. *Nat. Rev. Mater.* **2017**, *2*, 17024.
(17) Wang, P.; Bo, L.; Semenova, Y.; Farrell, G.; Brambilla, G. *Biosensors* **2015**, *5*, 471−499.
(18) Khalid, A.; Peng, L.; Arman, A.; Warren-Smith, S. C.; Schartner, E. P.; Sylvia, G. M.; Hutchinson, M. R.; Ebendorff-Heidepriem, H.; McLaughlin, R. A.; Gibson, B. C.; Li, J. *Sens. Actuators, B* **2020**, *311*, 127864.
(19) Zhou, W.; Li, K.; Wei, Y.; Hao, P.; Chi, M.; Liu, Y.; Wu, Y. *Biosens. Bioelectron.* **2018**, *106*, 99−104.
(20) Li, J.; Cui, D.; Jiang, Y.; Huang, J.; Cheng, P.; Pu, K. *Adv. Mater.* **2019**, *31*, 1905091.
(21) Xiao, A.; Huang, Y.; Zheng, J.; Chen, P.; Guan, B.-O. *ACS Appl. Mater. Interfaces* **2020**, *12*, 1799−1805.
(22) Guan, B.-O.; Huang, Y. *J. Lightwave Technol.* **2019**, *37*, 2616−2622.
(23) Yang, B.; Chen, Y.; Shi, J. *Chem* **2018**, *4*, 1284−1313.
(24) Li, H.; Huang, Y.; Chen, C.; Xiao, A.; Hou, G.; Huang, Y.; Feng, X.; Guan, B.-O. *Adv. Sci.* **2018**, *5*, 1701074.
(25) Shao, J.; Xie, H.; Huang, H.; Li, Z.; Sun, Z.; Xu, Y.; Xiao, Q.; Yu, X.-F.; Zhao, Y.; Zhang, H.; Wang, H.; Chu, P. K. *Nat. Commun.* **2016**, *7*, 12967.
(26) Tao, W.; Zhu, X.; Yu, X.; Zeng, X.; Xiao, Q.; Zhang, X.; Ji, X.; Wang, X.; Shi, J.; Zhang, H.; Mei, L. *Adv. Mater.* **2017**, *29*, 1603276.
(27) Chen, W.; Ouyang, J.; Liu, H.; Chen, M.; Zeng, K.; Sheng, J.; Liu, Z.; Han, Y.; Wang, L.; Li, J.; Deng, L.; Liu, Y.-N.; Guo, S. *Adv. Mater.* **2017**, *29*, 1603864.
(28) Sun, Q.; Ueno, K.; Yu, H.; Kubo, A.; Matsuo, Y.; Misawa, H. *Light: Sci. Appl.* **2013**, *2*, No. e118.
(29) Aksoy, İ.; Küçükkeçeci, H.; Sevgi, F.; Metin, Ö.; Patir, I. *ACS Appl. Mater. Interfaces* **2020**, *12*, 26822−26831.
(30) Nahta, R.; Yuan, L. X. H.; Zhang, B.; Kobayashi, R.; Esteva, F. J. *Cancer Res.* **2005**, *65*, 11118−11128.
(31) Xu, Y.; Ren, F.; Liu, H.; Zhang, H.; Han, Y.; Liu, Z.; Wang, W.; Sun, Q.; Zhao, C.; Li, Z. *ACS Appl. Mater. Interfaces* **2019**, *11*, 21399−21407.
(32) Sun, C.; Wen, L.; Zeng, J.; Wang, Y.; Sun, Q.; Deng, L.; Zhao, C.; Li, Z. *Biomaterials* **2016**, *91*, 81−89.
(33) Li, A.; Wang, Y.; Chen, T.; Zhao, W.; Zhang, A.; Feng, S.; Liu, J. *Eur. Polym. J.* **2017**, *92*, 51−60.
(34) Wang, Y.; Liu, X.; Deng, G.; Sun, J.; Yuan, H.; Li, Q.; Wang, Q.; Lu, J. *Nanoscale* **2018**, *10*, 2866−2875.
(35) Pasternack, R. M.; Amy, S.; Chabal, Y. J. *Langmuir* **2008**, *24*, 12963−12971.
(36) Yang, D.; Yang, G.; Yang, P.; Lv, R.; Gai, S.; Li, C.; He, F.; Lin, J. *Adv. Funct. Mater.* **2017**, *27*, 1700371.
(37) Fu, Y.; Wang, N.; Yang, A.; Law, H. K.-w.; Li, L.; Yan, F. *Adv. Mater.* **2017**, *29*, 1703787.
(38) Ali, M. A.; Mondal, K.; Jiao, Y.; Oren, S.; Xu, Z.; Sharma, A.; Dong, L. *ACS Appl. Mater. Interfaces* **2016**, *8*, 20570−20582.
(39) Wang, Y.; Ali, M. A.; Chow, E. K. C.; Dong, L.; Lu, M. *Biosens. Bioelectron.* **2018**, *107*, 224−229.
(40) Lou, J.; Wang, Y.; Tong, L. *Sensor* **2014**, *14*, 5823−5844.
(41) Huang, Y.; Xiao, A.; Hou, G.; Li, H.; Guo, T.; Guan, B.-O. *J. Mater. Chem. A* **2018**, *6*, 20513−20522.
(42) Zhu, M.; Cai, X.; Fujitsuka, M.; Zhang, J.; Majima, T. *Angew. Chem., Int. Ed.* **2017**, *56*, 2064−2068.
(43) Cai, X.; Mao, L.; Yang, S.; Han, K.; Zhang, J. *ACS Energy Lett.* **2018**, *3*, 932−939.
(44) Kim, E.; Baaske, M. D.; Vollmer, F. *Lab Chip* **2017**, *17*, 1190−1205.
(45) Gao, F.; Fan, T.; Wu, J.; Liu, S.; Du, Y.; Yao, Y.; Zhou, F.; Zhang, Y.; Liao, X.; Geng, D. *Biosens. Bioelectron.* **2017**, *96*, 62−67.
(46) Yang, H.-Y.; Shao, R.; Hung, M.-C.; Lee, M.-H. *Oncogene* **2001**, *20*, 3695−3702.
(47) Masters, J. R. *Nat. Rev. Cancer* **2002**, *2*, 315−319.
(48) Mass, R. D.; Press, M. F.; Anderson, S.; Cobleigh, M. A.; Vogel, C. L.; Dybdal, N.; Leiberman, G.; Slamon, D. J. *Clin. Breast Cancer* **2005**, *6*, 240−246.
(49) Alqarni, S. A.; Willmore, W. G.; Albert, J.; Smelser, C. W. *Appl. Opt.* **2021**, *60*, 2400−2411.

https://doi.org/10.1021/acs.analchem.2c01499
Anal. Chem. 2022, 94, 8058−8065